Draft: 2008 October 28

# Trigonometric Parallaxes of Massive Star Forming Regions: III. G59.7+0.1 and W 51 IRS2

Y. Xu[1,2], M. J. Reid[3], K. M. Menten[1], A. Brunthaler[1], X. W. Zheng[4], L. Moscadelli[5]


## ABSTRACT

We report trigonometric parallaxes for G59.7+0.1 and W 51 IRS2, corresponding to distances of $2.16^{+0.10}_{-0.09}$ kpc and $5.1^{+2.9}_{-1.4}$ kpc, respectively. The distance to G59.7+0.1 is smaller than its near kinematic distance and places it between the Carina-Sagittarius and Perseus spiral arms, probably in the Local (Orion) spur. The distance to W 51 IRS2, while subject to significant uncertainty, is close to its kinematic distance and places it near the tangent point of the Carina-Sagittarius arm. It also agrees well with a recent estimate based on O-type star spectro/photometry. Combining the distances and proper motions with observed radial velocities gives the full space motions of the star forming regions. We find modest deviations of 5 to 10 km s$^{-1}$ from circular Galactic orbits for these sources, both counter to Galactic rotation and toward the Galactic center.


*Subject headings:* techniques: interferometric — astrometry — galaxy: structure — stars: individual (G59.7+0.1, W 51 IRS2)

## 1. Introduction

We are carrying out a large project to study the spiral structure and kinematics of the Milky Way by measuring trigonometric parallaxes and proper motions of star forming regions. The target sources are 12 GHz methanol masers and we use the National Radio


[1]Max-Planck-Institut für Radioastronomie, Auf dem Hügel 69, 53121 Bonn, Germany

[2]Purple Mountain Observatory, Chinese Academy of Sciences, Nanjing 210008, China

[3]Harvard-Smithsonian Center for Astrophysics, 60 Garden Street, Cambridge, MA 02138, USA

[4]Nanjing University, Nanjing 20093, China

[5]Arcetri Obs., Firenze, Italy

Astronomy Observatory's [1] Very Long Baseline Array (VLBA). Details of this program can be found in Reid et al. (2008), hereafter called Paper I.

Here we present observations of G59.7+0.1 (IRAS 19410+2336) and W 51 IRS2. Depending on its distance, G59.7+0.1 could be in either the Carina-Sagittarius or Local spiral arm of the Milky Way. W 51 IRS2 is a very well studied region of high-mass star formation; its radial velocity is very close to the maximum allowed by circular rotation for standard models of the Milky Way, and it has generally been assigned the tangent-point distance, $D$, in the Carina-Sagittarius arm. Our direct measurements of distance and proper motion indicate the true location of these star forming regions in the Galaxy and their departures from circular Galactic orbits.

## 2. Observations and Calibration

We conducted phase-referenced observations of G59.7+0.1 and W 51 IRS2 with respect to two extragalactic radio sources with the VLBA under program BR100D in order to measure parallaxes. Paper I describes the general observational setup and data calibration procedures, so here we only describe details specific to the observations of G59.7+0.1 and W 51 IRS2.

The time between epochs was planned to be three months, matching the eastward and northward extrema of the Earth's orbit as seen by the sources. The observations were conducted on 2005 Jul. 13 and Oct. 20, 2006 Jan 15, Apr. 23 and Oct. 19, and 2007 Apr. 19. However, the data for the epoch of 2006 Apr. 23 were not correlated at the position of W 51 IRS2 and were lost for this source.

Background compact extragalactic sources were chosen as follows. For G59.7+0.1, we selected J1946+2300 (with separation of 1.0° from the maser target) from the ICRF source list (Ma et al. 1998) and J1941+2307 (separation 0.7°) and J1943+2330 (separation 0.3°), based on a VLA survey of compact NVSS sources (Xu et al. 2006a). Ultimately, we used only data from the first two sources, as we failed to detect J1943+2330. For W 51 IRS2, we chose two sources from the VLBA Calibrator Survey (Petrov et al. 2006), J1922+1530 (separation 1.0°) and J1924+1540 (separation 1.2°), augmented by J1922+1504 (separation 0.6°), which was found in our VLA survey. Two strong sources (J1800+3848 and J1922+1530) were observed near the beginning, middle and end of the observations in order to monitor

[1] The National Radio Astronomy Observatory is a facility of the National Science Foundation operated under cooperative agreement by Associated Universities, Inc.

delay and electronic phase differences among the IF bands.

After applying the basic calibration procedures described in Paper I, we used the maser features toward G59.7+0.1 at $V_{\rm LSR}$ = 27.4 km s$^{-1}$ and toward W 51 IRS2 at $V_{\rm LSR}$ = 56.4 km s$^{-1}$ for interferometer phase-reference data. When imaging the data referenced to G59.7+0.1, we adopted a round restoring beam of 1.7 mas (FWHM), slightly larger than the geometric mean of the interferometer response ("dirty beam") of $1.7 \times 1.1$ mas at a position angle of 14° East of North. For the data referenced to W 51 IRS2, we adopted a round restoring beam of 3.3 mas (FWHM), slightly larger than the dirty beam of $3.3 \times 1.5$ mas at a position angle of 134°.

## 3. Parallax and Proper Motion

### 3.1. G59.7+0.1

A map of the maser emission made by integrating all channels with detectable emission at the first epoch is shown in Fig. 1. Millimeter and centimeter wavelength continuum data associated with the maser are also presented. We analyzed 8.4 GHz data, which we obtained from the VLA archival database, and find a weak continuum source with flux density of $0.77 \pm 0.18$ mJy at $(\alpha_{J2000}, \delta_{J2000})$ = (19 43 11.21, +23 44 03.32), with a probable position uncertainty of about 0.2 arcsec. We conclude that the methanol maser (Table 1) and the compact continuum sources are associated. The continuum source has an upper limit of $\approx 2''$ for its size. One millimeter wavelength core is also associated with the maser and the weak cm continuum source (Beuther, Schilke & Stanke 2003).

We show the first epoch images of each background continuum source in Fig. 2. One can see that they both appear dominated by a single compact component.

When conducting phase-referenced observations, it is important that the position of the reference source matches the interferometer phase center in order to minimize second-order positional errors and improve image quality. Since the ICRF source J1946+2300 has a position accuracy of $\approx 1$ mas, we used its position as the basis for all absolute positions given in Table 1.

We fitted elliptical Gaussian brightness distributions to two maser spots and the two background radio sources for all seven epochs. In Fig. 3, we plot the positions of two maser spots (at $V_{\rm LSR}$ of 26.6 and 27.4 km s$^{-1}$) relative to two background sources. The measured positions of the G59.7+0.1 masers were then modeled as a linear combination of the elliptical parallax and linear proper motion signatures. Because systematic errors

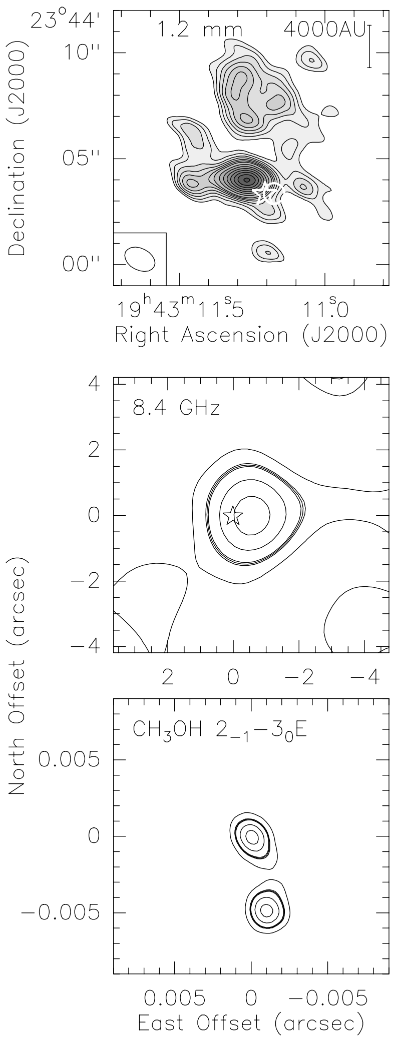


Fig. 1.— *Upper Panel*: Continuum emission at 250 GHz (*contours*) imaged with the IRAM Plateau de Bure interferometer (Beuther, Schilke & Stanke 2003). The the star marks the 12.2 $CH_3OH$ maser position (see Table 1). *Middle Panel*: Weak 8.4 GHz emission toward G59.7+0.1 imaged with the VLA. Contours represent 30, 50, 70, and 90% of the peak brightness of 0.68 mJy beam$^{-1}$. The lowest contour represents 2 times the rms noise level, while the *thick* 50% contour closely follows the size of the synthesized beam ($2.9'' \times 2.4''$). The (0,0) position corresponds to the position of the 12 GHz methanol maser. *Bottom panel*: Map made by integrating all channels with detectable methanol maser emission at the first epoch. The $V_{\rm LSR}$ = 27.4 km s$^{-1}$ maser spot, located at the origin, was used for the parallax fits. The maser spot located near $(-0.001, -0.005)$ is at $V_{\rm LSR}$ = 26.6 km s$^{-1}$. Contours represent 30, 50 (bold), 70, and 90% of the velocity-integrated flux density of 0.82 Jy km s$^{-1}$. The restoring beam is 1.7 mas FWHM for the maser image.

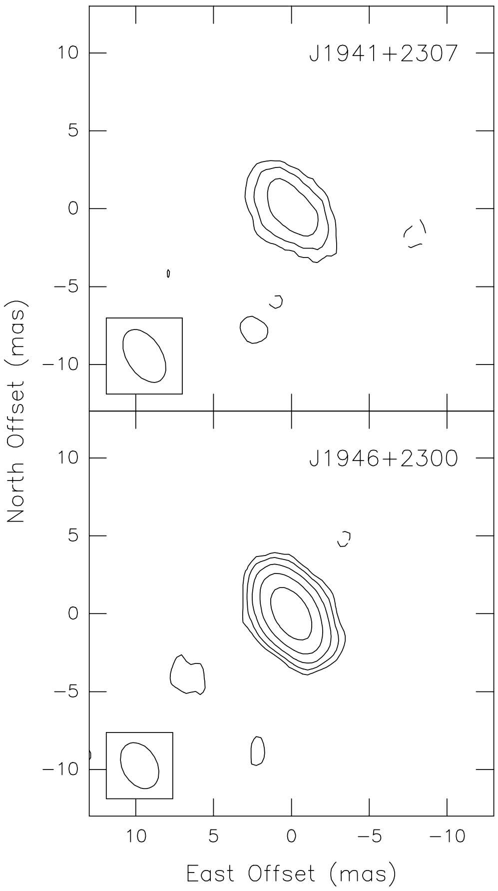


Fig. 2.— First epoch images of the two background sources phase-referenced to the G59.7+0.1 methanol maser. For both sources the lowest negative (*dashed*) and positive (*solid*) contours are 4 times the rms noise level, which is 0.4 mJy beam$^{-1}$ for J1941+2307 (upper panel) and 0.7 mJy beam$^{-1}$ for J1946+2300 (lower panel). Other contours represent increases by a factor of 2 starting from that level. The peak brightness and integrated flux density are 10.8 mJy beam$^{-1}$ and 16.3 mJy, respectively, for J1941+2307 and 74.8 mJy beam$^{-1}$ and 114 mJy, respectively, for J1946+2300. The upper limit of source sizes is 3.0 mas for J1941+2307 and 2.9 mas for J1946+2300. The FWHM of the synthesized beams are represented in the lower left corner of each panel.

(owing to small uncompensated atmospheric delays and, in some cases, varying maser source structure) typically dominate over signal to noise considerations when measuring relative source positions, we added "error floors" in quadrature to the formal position uncertainties. We used different error floors for the Right Ascension and Declination data and adjusted them to yield post-fit residuals with $\chi^2$ per degree of freedom near unity for both coordinates. Individual fits are given in Table 2.

Fitting for the parallax and proper motion for both sources simultaneously, we obtain $\pi = 0.463 \pm 0.020$ mas. The quoted parallax uncertainty is the formal fitting uncertainty, multiplied by $\sqrt{2}$ to account for possible correlations between the position data for the two maser spots. This parallax corresponds to a distance of $2.16^{+0.10}_{-0.09}$ kpc, which is smaller than the "near" kinematic distance of 2.7 kpc, and rules out the far distance of 5.8 kpc. The average proper motions in the eastward and northward directions are $-1.65 \pm 0.03$ and $-5.12 \pm 0.08$ mas y$^{-1}$, respectively, as listed in Table 2. Similarly, the uncertainties were also multiplied by $\sqrt{2}$.

### 3.2. W 51 IRS2

We made a 12 GHz methanol maser map of W 51 IRS2 by integrating all channels with detectable emission at the first epoch. This map is shown in Fig. 4, superposed on a continuum (23.8 GHz) image from archival VLA data (AS724).

In Fig. 5, we show maps of the background continuum sources, phase referenced to the $V_{\rm LSR} = 56.4$ km s$^{-1}$ maser spot in W 51 IRS2, from the first epoch. These background sources are dominated by a single compact component. Absolute positions for the maser reference spot and the background sources are given in Table 1. These are based on the position of J1924+1540, which is uncertain by $\approx 1$ mas (Petrov et al. 2006).

In order to determine the parallax and proper motion of W 51 IRS2, we used positions of two strong maser spots relative to all three background sources. Following the fitting procedures discussed for G59.7+0.1, individual spot/background source parallax solutions are listed in Table 3. A combined parallax solution yielded $\pi = 0.195 \pm 0.071$ mas, corresponding to a distance of $5.1^{+2.9}_{-1.4}$ kpc, which will be discussed in §3.3. The data and model used for this fit are shown in Fig. 6. The formal parallax uncertainty has been multiplied by $\sqrt{2}$, in order to account for possible correlations between the position data for the two maser spots. Some of the relative positions for the fifth epoch (2006.80) appear to be outliers. Were we to drop the data from this epoch, the parallax estimate decreases to $\pi = 0.166 \pm 0.069$ mas, suggesting a slightly greater distance. The average proper motions of the two maser spots in the

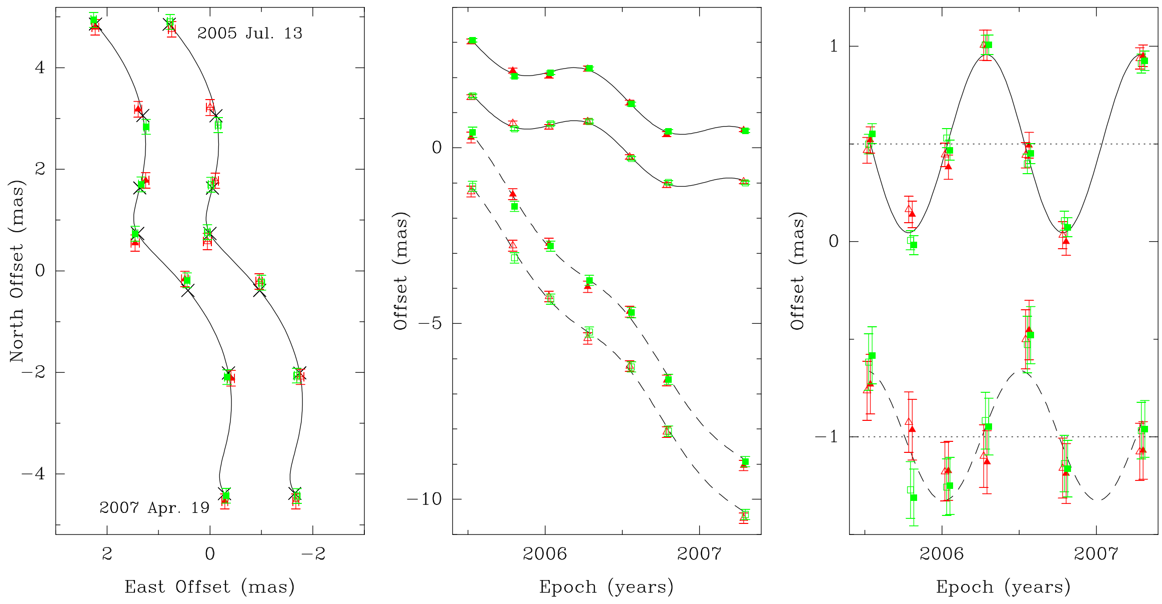


Fig. 3.— Parallax and proper motion data and fits for G59.7+0.1. Plotted are position measurements of two maser spots at $V_{\rm LSR} = 27.4$ and 26.6 km s$^{-1}$ *(open and solid symbols)* in G59.7+0.1 relative to two background sources: J1941+2307 *(red triangles)* and J1946+2300 *(green squares)*. *Left Panel:* Positions on the sky with first and last epochs labeled. The expected positions from the parallax and proper motion fit are indicated *(crosses)*. *Middle Panel:* Eastward *(solid lines)* and northward *(dashed lines)* positions and best fit parallax and proper motions fits versus time. *Right Panel:* Same as the *middle panel*, except the best fit proper motions have been removed, allowing all data to be overlaid and the effects of only the parallax seen.

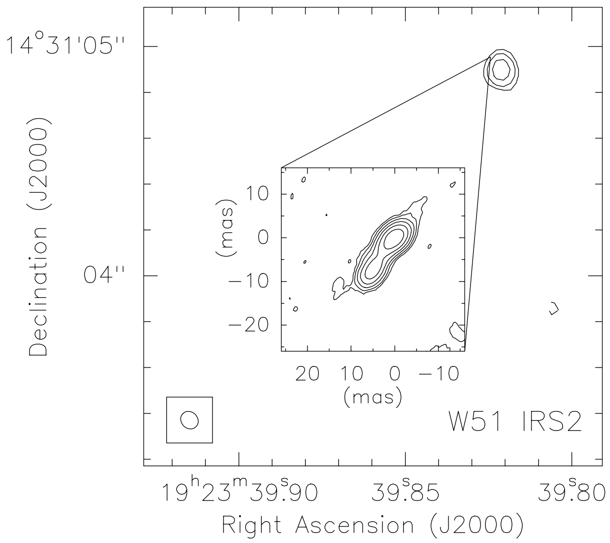


Fig. 4.— The large image shows weak 23.8 GHz continuum emission from a hypercompact HII region south of W 51 d, the ultracompact HII region associated with W 51 IRS2. The image was produced from archival VLA with a restoring beam (indicated in the lower left corner) of ≈ 0.″08. Contours are -5, 5, 10, and 20 times the rms noise of 0.28 mJy beam$^{-1}$. The methanol maser is, as indicated, clearly associated with the hypercompact HII region. The separation between them is around 0.07 arcsec. The inset shows the velocity-integrated methanol maser emission with contours representing 5, 10, 20, 40, 80, and 160 times 5 mJy beam$^{-1}$ km s$^{-1}$. The x- and y-axes give east and west offset, respectively, relative to the position given in Table 1.

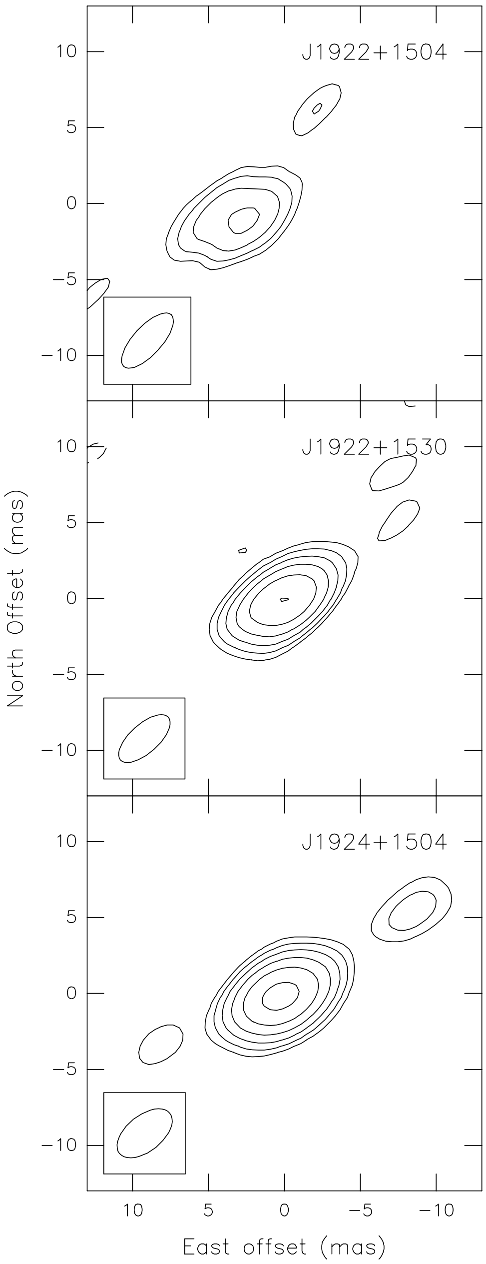


Fig. 5.— First epoch images of of the three background sources phase-referenced to the W 51 IRS 2 methanol maser. For all sources the lowest negative and positve contours are 4 times the rms noise level, which is 0.6 mJy beam$^{-1}$ for J1922+1530 (top panel), 1.8 mJy beam$^{-1}$ for J1922+1504 (middle panel) and 2.9 mJy beam$^{-1}$ for J1924+1540 (bottom panel). Other contours represent increases by a factor of 2 starting from that level. The peak brightness and integrated flux density are 22.5 mJy beam$^{-1}$ and 43 mJy, respectively, for J1922+1530, 24 mJy beam$^{-1}$ and 37 mJy, respectively, for J1922+1504, and 465 mJy beam$^{-1}$ and 615 mJy, respectively, for J1924+1504. The upper limit of source sizes is 2.6 mas for J1922+1530, 3.8 mas for J1922+1504, and 0.0 mas for J1924+1504. The FWHM of the synthesized beams are represented in the lower left corner of each panel.

eastward and northward directions are $-2.49 \pm 0.08$ and $-5.51 \pm 0.11$ mas $y^{-1}$, respectively, as listed in Table 3.

### 3.3. The Distance to W 51 IRS 2

It is interesting to compare our directly measured distance of $5.1^{+2.9}_{-1.4}$ kpc with other distance determinations that have recently published for W51 IRS 2. Imai et al. (2002) performed multi-epoch VLBI observations of the intense $H_2O$ maser outflow in the region ("W 51 N"). A kinematic model they fitted to the measured internal proper motions of the outflow contains its distance as free parameter, for which they find a best fit value of $6.1 \pm 1.3$ kpc.

Barbosa et al. (2008) combine near infrared spectroscopy and radio continuum and recombination line observations to characterize the exciting star of W 51 IRS 2. Using available data and calculations modeling the temperatures, radii and Lyman continuum production rates of Zero Age Main Sequence (ZAMS) stars, they propose a classification of its spectral type as O3 or O4 (ZAMS). Using the source's observed bolometric luminosity, they derive $D = 5.1$ and 5.8 kpc for these two choices, respectively, which compares very well with our distance.

We note that the same group recently also obtained a distance of $2.0 \pm 0.3$ from spectroscopic and photometric observations of four objects in W 51 A classified as O-type stars (Figueredo et al. 2008). W 51 A and W 51 IRS 2, separated by an angle of roughly 1 arc minute (or 1.5 pc), are commonly thought to belong to the same complex and a (near) kinematic distance of 5.5 kpc has been found by Russeil (2003) for W 51 A, comparable to our parallax distance of IRS 2.

Currently, large-scale infrared surveys are leading to the discovery of many new open star clusters throughout the Milky Way (see, e.g., Ivanov et al. 2002; Dutra et al. 2003; Bica et al. 2003), why may trigger a renaissance in efforts to use spectro/photometry of O-type stars for distance estimates with the goal of constraining Galactic structure (see, e.g., Messineo et al. 2006). In view of this, we find that the discrepancy discussed above deserves further investigation. We note that in the famous case of W3OH in the Perseus arm, the O-star method yielded $D = 2.3$ kpc for the close-by Per OB 1 association (Humphreys 1978), roughly half the kinematic distance implied by a model of Galactic rotation. This turned out to be in excellent agreement with the 2.0 kpc directly determined via two VLBI parallax measurements of $CH_3OH$ and $H_2O$ masers in W3OH much later (Hachisuka et al. 2006; Xu et al. 2006b). Future maser VLBI trigonometric parallax measurements of W 51

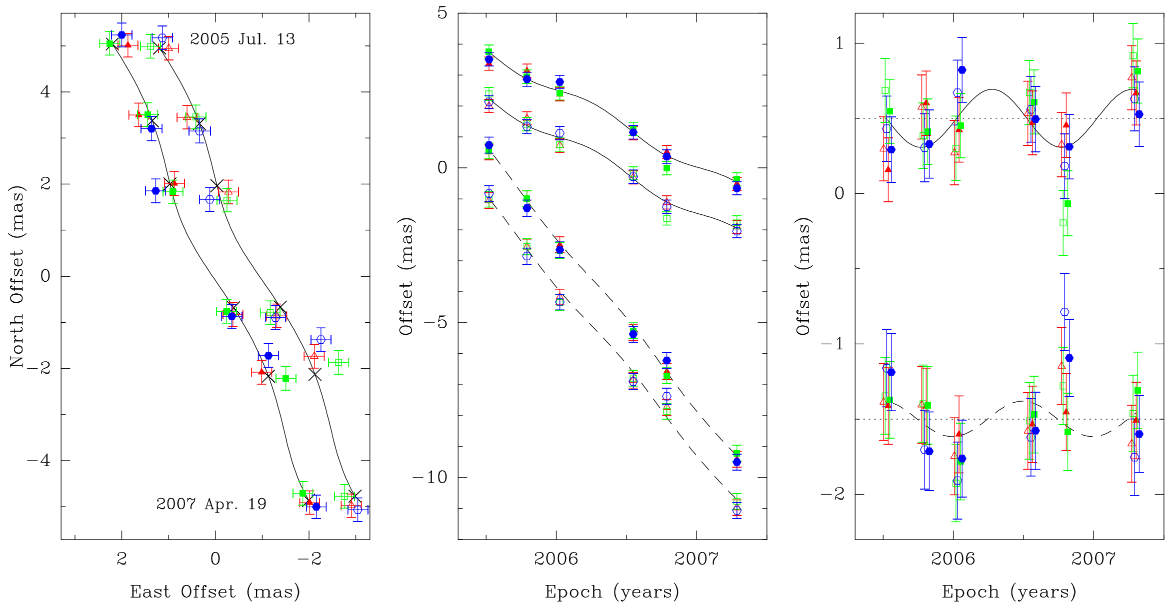


Fig. 6.— Parallax and proper motion data and fits for W 51 IRS2. Plotted are position measurements of two maser spots at $V_{\rm LSR}$ = 56.0 and 56.4 km s$^{-1}$ *(open and solid symbols)* relative to the three background sources: J1922+1504 *(blue hexagons)*, J1922+1530 *(red triangles)* and J1924+1540 *(green squares)*. *Left Panel:* Positions on the sky with first and last epochs labeled. Data for the two maser spots are offset horizontally for clarity. The expected positions from the parallax and proper motion fit are indicated *(crosses)*. *Middle Panel:* Eastward *(solid lines)* and North *(dashed lines)* positions and best fit parallax and proper motions fits versus time. Data for the two maser spots are offset vertically and small time shifts have been added to the data for clarity *Right Panel:* Same as the *middle panel*, except the with the best fit proper motions have been removed, allowing all data to be overlaid and the effects of only the parallax seen.

A could certainly contribute to the perplexing question described above.

### 3.4. Galactic Locations and 3-D Motions

In order to study the 3-dimensional motion of the maser sources in the Galaxy, we converted the proper motions and radial velocities to a Galactocentric reference frame. We adopt the IAU standard constants of $R_0 = 8.5$ kpc and $\Theta_0 = 220$ km s$^{-1}$, and the Hipparcos Solar Motion values $U = 10.0 \pm 0.40$, $V = 5.25 \pm 0.60$, and $W = 7.17 \pm 0.40$ km s$^{-1}$ from Dehnen & Binney (1998). For these values and a flat rotation curve for the Galaxy, the Galactocentric distance of G59.7+0.1 is 7.64 kpc. Its velocity in the direction of Galactic rotation is $10 \pm 3$ km s$^{-1}$ slower than for a circular orbit. Its velocity toward the Galactic Center is $7 \pm 1$ km s$^{-1}$, and its velocity toward North Galactic Pole is $-4 \pm 1$ km s$^{-1}$. These uncertainties include measurement errors, but do not include systematic terms from uncertainty in $R_0$ and $\Theta_0$. Thus we find that G59.7+0.1 has a peculiar motion of $\approx 12$ km s$^{-1}$ directed mostly counter to Galactic rotation and toward the Galactic Center.

Our trigonometric parallax places G59.7+0.1 in the Milky Way between the Carina-Sagittarius and Perseus spiral arms. It seems to be a fairly distant member of the Local (Orion) arm or spur, located close to the point where the spur joins the Carina-Sagittarius arm. G59.7+0.1 is near the open cluster NGC 6823, which is also thought to be located in the Local arm (Basharina, Pavlovskaya & Filippova 1980). Spur-like structures have been observed for many galaxies (Aalto et al. 1999; Scoville et al. 2001; La Vigne, Vogel & Ostriker 2006). These spurs may form as a consequence of gravitational instabilities inside spiral arms or/and effects of magnetic fields (Balbus 1998; Kim & Ostriker 2002; Shetty & Ostriker 2006). Kim & Ostriker (2002) showed that the growth of spurs can occur due to the mutual contributions of self-gravity and magnetic fields via the so-called magneto-Jeans instability.

Adopting a distance of 5.1 kpc from the Sun, places W 51 IRS2 6.5 kpc from the Galactic center, in the the Carina-Sagittarius spiral arm and reasonably close the spiral arm tangent point. Converting the proper motions and radial velocity of W 51 IRS2 to a Galactocentric reference frame, we find a velocity in the direction of Galactic rotation that is $5 \pm 10$ km s$^{-1}$ slower than for a circular orbit. Its velocity toward the Galactic Center is $21 \pm 15$ km s$^{-1}$, and its velocity toward North Galactic Pole is $-3 \pm 5$ km s$^{-1}$. These peculiar motion uncertainties are fairly large, primarily because of the uncertain parallax measurement.

## 4. Conclusions

We have measured the parallax and proper motion of methanal masers in two regions of high-mass star formation. G59.7+0.1 lies at a distance of $2.16^{+0.10}_{-0.09}$ kpc in the Local (Orion) arm or spur. Its space motion, relative to a frame rotating with the Milky Way, is about 12 km $s^{-1}$ counter to Galactic rotation and toward the Galactic center. Our parallax for W 51 IRS2, while less accurate than for G59.7+0.1, indicates that W 51 IRS2 is in the Carina-Sagittarius spiral arm.

This work was supported by Chinese NSF through grants NSF 10673024, NSF 10733030, NSF 10703010 and NSF 10621303, and NBRPC (973 Program) under grant 2007CB815403. Andreas Brunthaler was supported by the DFG Priority Programme 1177.

*Facilities:* VLBA

## REFERENCES

Aalto, S., Hüttemister, S., Scoville, N. Z. & Thaddeus, P. 1999, ApJ, 522, 165

Balbus, S. A. 1988, ApJ, 324, 60

Barbosa, C. L., Blum, R. D., Conti, P. S., Damineli, A., & Figuerêdo, E. 2008, ApJ, 678, L55

Beuther, H., Schilke, P. & Stanke, T. 2003, A&A, 408, 601

Basharina, T. S., Pavlovskaya, E. D., & Filippova, A. A. 1980, *SvA*, 24, 559

Dutra, C. M., Bica, E., Soares, J., & Barbuy, B. 2003, A&A, 400, 533

Bica, E., Dutra, C. M., Soares, J., & Barbuy, B. 2003, A&A, 404, 223

Dehnen, W., & Binney, J. J., 1998, MNRAS, 298, 387

Figurêdo, E., Blum, R. D., Damineli, A., Conti, P. S. & Barbosa, C. L. 2008, AJ, 136, 221

Hachisuka, K., Brunthaler, A., Menten, K. M., Reid, M. J. et al. 2006, ApJ, 645, 337

Humphreys, R. M. 1978, ApJS, 38, 309

Imai, H., Watanabe, T., Omodaka, T., Nishio, M., Kameya, O., Miyaji, T., & Nakajima, J. 2002, PASJ, 54, 741

Ivanov, V. D., Borissova, J., Pessev, P., Ivanov, G. R., & Kurtev, R. 2002, A&A, 394, L1

Kim, W.-T., & Ostriker, E. C. 2002, ApJ, 570, 132

La Vigne, M. A., Vogel, S. N., & Ostriker, E. C. 2006, ApJ, 650, 818

Ma, C. et al. 1998, AJ, 116, 516

Messineo, M., Petr-Gotzens, M., Menten, K. M., Schuller, F., & Habing, H. J. 2006, Journal of Physics Conference Series, 54, 238

Petrov, L., Kovalev, Y. Y., Fomalont, E., & Gordon. D. 2006, AJ, 131, 1872

Reid, M. J. et al. 2008, submitted to ApJ, (Paper I).

Russeil, D. 2003, A&A, 397, 133

Scoville, N. Z., Polletta, M., Ewald, S., Stolovy, S. R., Thompson, R., & Rieke, M. 2001 AJ, 122, 3017

Shetty, R. & Ostriker, E. C. 2006, ApJ, 647, 997

Xu, Y., Reid, M. J., Menten, K. M. & Zheng, X. W. 2006a, ApJS, 166, 526

Xu, Y., Reid, M. J., Zheng, X. W., & Menten, K. M. 2006b, Science, 311, 54

---

Table 1. Positions and Brightness

| Source | R.A. (J2000) ($^{h}$ $^{m}$ $^{s}$) | Dec. (J2000) ($^\circ$ $'$ $''$) | $\phi$ ($^\circ$) | Brightness (Jy/beam) | $V_{\rm LSR}$ (km s$^{-1}$) | Restoring Beam (mas, mas, deg) |
|---|---|---|---|---|---|---|
| G59.7+0.1 ...... | 19 43 11.2470 | 23 44 03.315 | | 1.4 | 27.4 | 1.7 |
| J1946+2300 ...... | 19 46 06.25140 | 23 00 04.4145 | 1.0 | 0.073 | | 2.2×3.2 @ 33 |
| J1941+2307 ....... | 19 41 55.1114 | 23 07 56.525 | 0.7 | 0.010 | | 2.3×3.8 @ 30 |
| | | | | | | |
| W51 ......... | 19 23 39.8244 | 14 31 04.953 | | 2.2 | 56.4 | 3.3 |
| J1924+1540 ... | 19 24 39.45588 | 15 40 43.9417 | 1.2 | 0.46 | | 2.4×4.3 @ -51 |
| J1922+1530 ... | 19 22 34.6993 | 15 30 10.0327 | 1.0 | 0.23 | | 1.9×4.2 @ -48 |
| J1922+1504 ... | 19 22 33.2728 | 15 04 47.537 | 0.6 | 0.022 | | 1.9×4.6 @ -43 |

Note. — $\phi$ is the separations. The radial velocity of the masers and the size and shape of the interferometer restoring beam are listed for the first epoch's data. The position angle of the beam is defined as East of North.

Table 2. G59.7+0.1 Parallax & Proper Motion Fit

| Maser $V_{\rm LSR}$ (km s$^{-1}$) | Background Source | Parallax (mas) | $\mu_x$ (mas y$^{-1}$) | $\mu_y$ (mas y$^{-1}$) |
|---|---|---|---|---|
| 26.6 ...... | J1941+2307 | $0.459 \pm 0.043$ | $-1.68 \pm 0.06$ | $-5.18 \pm 0.12$ |
| 26.6 ...... | J1946+2300 | $0.484 \pm 0.025$ | $-1.68 \pm 0.03$ | $-5.09 \pm 0.10$ |
| 27.4 ...... | J1941+2307 | $0.436 \pm 0.036$ | $-1.63 \pm 0.04$ | $-5.17 \pm 0.11$ |
| 27.4 ...... | J1946+2300 | $0.466 \pm 0.027$ | $-1.63 \pm 0.04$ | $-5.08 \pm 0.08$ |
| | | | | |
| 26.6 ...... | combined | $0.463 \pm 0.020$ | $-1.68 \pm 0.03$ | $-5.13 \pm 0.08$ |
| 27.4 ...... | | | $-1.63 \pm 0.03$ | $-5.12 \pm 0.07$ |

Note. — Combined fit used a single parallax parameter for both maser spots relative to the two background sources; a single proper motion was fit for each maser spot relative to all two background sources.

Table 3. W51 Parallax & Proper Motion Fit

| Maser $V_{\mathrm{LSR}}$ (km s$^{-1}$) | Background Source | Parallax (mas) | $\mu_x$ (mas y$^{-1}$) | $\mu_y$ (mas y$^{-1}$) |
|---|---|---|---|---|
| 56.0 ...... | J1922+1504 | $0.240 \pm 0.078$ | $-2.54 \pm 0.09$ | $-5.45 \pm 0.33$ |
| 56.0 ...... | J1922+1530 | $0.055 \pm 0.111$ | $-2.33 \pm 0.13$ | $-5.49 \pm 0.17$ |
| 56.0 ...... | J1924+1540 | $0.377 \pm 0.149$ | $-2.60 \pm 0.20$ | $-5.42 \pm 0.17$ |
| 56.4 ...... | J1922+1504 | $0.155 \pm 0.127$ | $-2.51 \pm 0.15$ | $-5.56 \pm 0.21$ |
| 56.4 ...... | J1922+1530 | $0.023 \pm 0.062$ | $-2.33 \pm 0.12$ | $-5.60 \pm 0.05$ |
| 56.4 ...... | J1924+1540 | $0.317 \pm 0.094$ | $-2.59 \pm 0.13$ | $-5.52 \pm 0.10$ |
| 56.0 ...... | combined | $0.195 \pm 0.071$ | $-2.49 \pm 0.07$ | $-5.45 \pm 0.14$ |
| 56.4 ...... | | | $-2.48 \pm 0.08$ | $-5.56 \pm 0.08$ |

Note. — Combined fit used a single parallax parameter for both maser spots relative to the three background sources; a single proper motion was fit for each maser spot relative to all three background sources.